Interdependent Nutrient Availability and Steroid Hormone Signals Facilitate Root Growth Plasticity

Amar Pal Singh, Yulia Fridman, Neta Holland, Michal Ackerman-Lavert, Rani Zananiri, Yvon Jaillais, Arnon Henn, Sigal Savaldi-Goldstein

Article

Developmental Cell

Interdependent Nutrient Availability and Steroid Hormone Signals Facilitate Root Growth Plasticity

Graphical Abstract

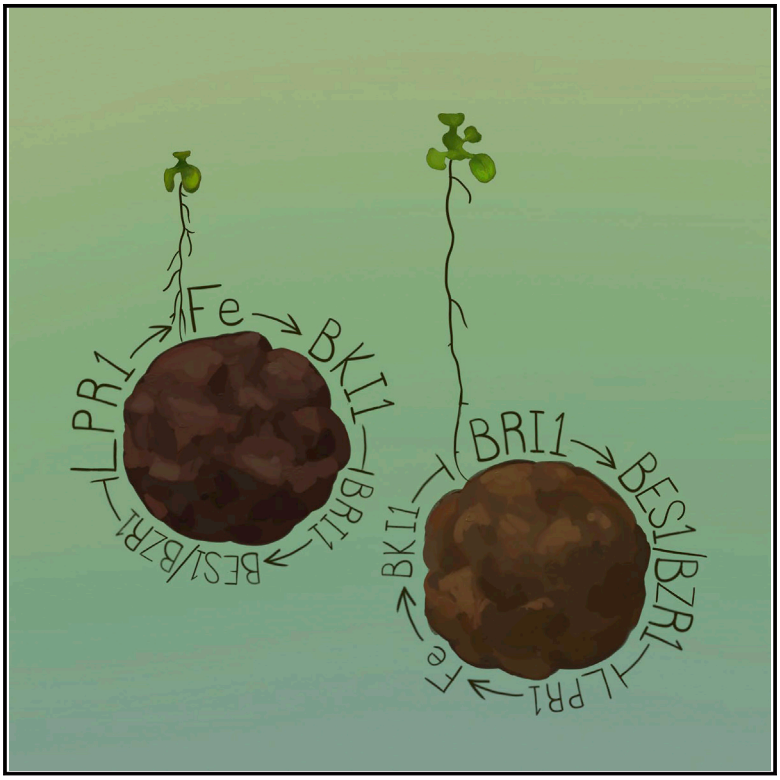

Authors

Amar Pal Singh, Yulia Fridman, Neta Holland, ..., Yvon Jaillais, Arnon Henn, Sigal Savaldi-Goldstein

Correspondence

sigal@technion.ac.il

In Brief

Plants adapt to changes in nutrient availability by modulating the morphology of their roots. Singh et al. show that phosphate and iron levels modulate the brassinosteroid signaling pathway. In turn, brassinosteroid activity controls iron accumulation in elongating cells. This interdependent interaction determines the extent of root elongation.

Highlights

- BKI1 is an integrator of Pi and iron cues in brassinosteroid signaling
- Low iron promotes root growth by activating brassinosteroid signaling
- BZR1 prevents low-Pi-mediated iron accumulation by repressing LPR1

Singh et al., 2018, Developmental Cell *46*, 59–72
July 2, 2018
https://doi.org/10.1016/j.devcel.2018.06.002

CellPress

Developmental Cell
Article

Interdependent Nutrient Availability and Steroid Hormone Signals Facilitate Root Growth Plasticity

Amar Pal Singh,[1,3] Yulia Fridman,[1] Neta Holland,[1] Michal Ackerman-Lavert,[1] Rani Zananiri,[1] Yvon Jaillais,[2] Arnon Henn,[1] and Sigal Savaldi-Goldstein[1,4,*]
[1]Faculty of Biology, Technion-Israel Institute of Technology, Haifa 3200003, Israel
[2]Laboratoire Reproduction et Développement des Plantes, Université de Lyon, ENS de Lyon, UCB Lyon 1, CNRS, INRA, 69342 Lyon, France
[3]Present address: National Institute of Plant Genome Research, Aruna Asaf Ali Marg, New Delhi 110067, India
[4]Lead Contact
*Correspondence: sigal@technion.ac.il
https://doi.org/10.1016/j.devcel.2018.06.002

SUMMARY

Plants acquire essential elements from inherently heterogeneous soils, in which phosphate and iron availabilities vary. Consequently, plants have developed adaptive strategies to cope with low iron or phosphate levels, including alternation between root growth enhancement and attenuation. How this adaptive response is achieved remains unclear. Here, we found that low iron accelerates root growth in *Arabidopsis thaliana* by activating brassinosteroid signaling, whereas low-phosphate-induced high iron accumulation inhibits it. Altered hormone signaling intensity also modulated iron accumulation in the root elongation and differentiation zones, constituting a feedback response between brassinosteroid and iron. Surprisingly, the early effect of low iron levels on root growth depended on the brassinosteroid receptor but was apparently hormone ligand-independent. The brassinosteroid receptor inhibitor BKI1, the transcription factors BES1/BZR1, and the ferroxidase LPR1 operate at the base of this feedback loop. Hence, shared brassinosteroid and iron regulatory components link nutrient status to root morphology, thereby driving the adaptive response.

INTRODUCTION

Optimal plant growth and development depend on the ability to cope with adverse environmental conditions, such as limited mineral nutrient availability in soil (Lynch, 1995). As such, plants sense external and internal concentrations of minerals and adjust their root system architecture and root growth rate accordingly (Gruber et al., 2013). One example of this growth plasticity is the local sensing of low phosphate (Pi) availability by the *Arabidopsis* root tip (Svistoonoff et al., 2007). The response involves inhibition of primary root elongation due to rapid impairment of cell elongation, followed by impairment of meristem maintenance after days (Hanlon et al., 2018; Balzergue et al., 2017; Gutierrez-Alanis et al., 2017; Müller et al., 2015; Svistoonoff et al., 2007; Sanchez-Calderon et al., 2005). In parallel, the density and length of lateral roots and root hairs are enhanced, resulting in an overall adaptive switch (Ruiz Herrera et al., 2015; Williamson et al., 2001). This kind of morphological change, that may also involve a change in root growth angle, is thought to enable efficient absorption of Pi from topsoil, where it is more available (Lynch, 2011). These low-Pi-mediated morphological changes also depend on iron (Fe) availability (Ward et al., 2008; Svistoonoff et al., 2007). If Fe is available, low Pi triggers high accumulation of apoplastic Fe (mainly ferric Fe, Fe^{3+} but also ferrous Fe, Fe^{2+}) in the elongation zone (Balzergue et al., 2017) and in the quiescent center (QC) cells that compose the stem cell niche (Müller et al., 2015). The cell-wall-targeted ferroxidases *Low Phosphate Root (LPR) 1* and *2* promote this accumulation of Fe through a yet unknown mechanism (Müller et al., 2015). Loss-of-function mutant in LPR1 is insensitive to low Pi (Ticconi et al., 2009; Svistoonoff et al., 2007), and LPR1 overexpression leads to ectopic Fe accumulation in response to low Pi conditions (Müller et al., 2015). Few components acting upstream of LPR1 were identified (Balzergue et al., 2017; Dong et al., 2017; Mora-Macias et al., 2017; Ticconi et al., 2009); however, how LPR1 is regulated by low Pi levels remains unclear. Under conditions of complete Fe depletion (and adequate Pi levels), root growth is inhibited. Interestingly, mild Fe deficiency (hereafter referred as low Fe) has a root growth-promoting effect (Gruber et al., 2013). Currently, nothing is known about how root growth is promoted by low Fe.

The steroid hormone brassinosteroid (BR) pathway controls root growth in a dose-dependent and tissue-dependent manner (Singh and Savaldi-Goldstein, 2015). Roots of BR-deficient mutants are short, with small cells and reduced duration of meristematic cell proliferation (Gonzalez-Garcia et al., 2011; Hacham et al., 2011). Supra-optimal levels of the hormone, as with exogenous application of BRs, inhibit root elongation due to early differentiation of meristematic cells (Gonzalez-Garcia et al., 2011; Mussig et al., 2003). BR activates the pathway by binding to the extracellular domain of its primary receptor BRASSINOSTEROID INSENSITIVE1 (BRI1) and its co-receptor BRI1-ASSOCIATED KINASE 1 (BAK1) (Santiago

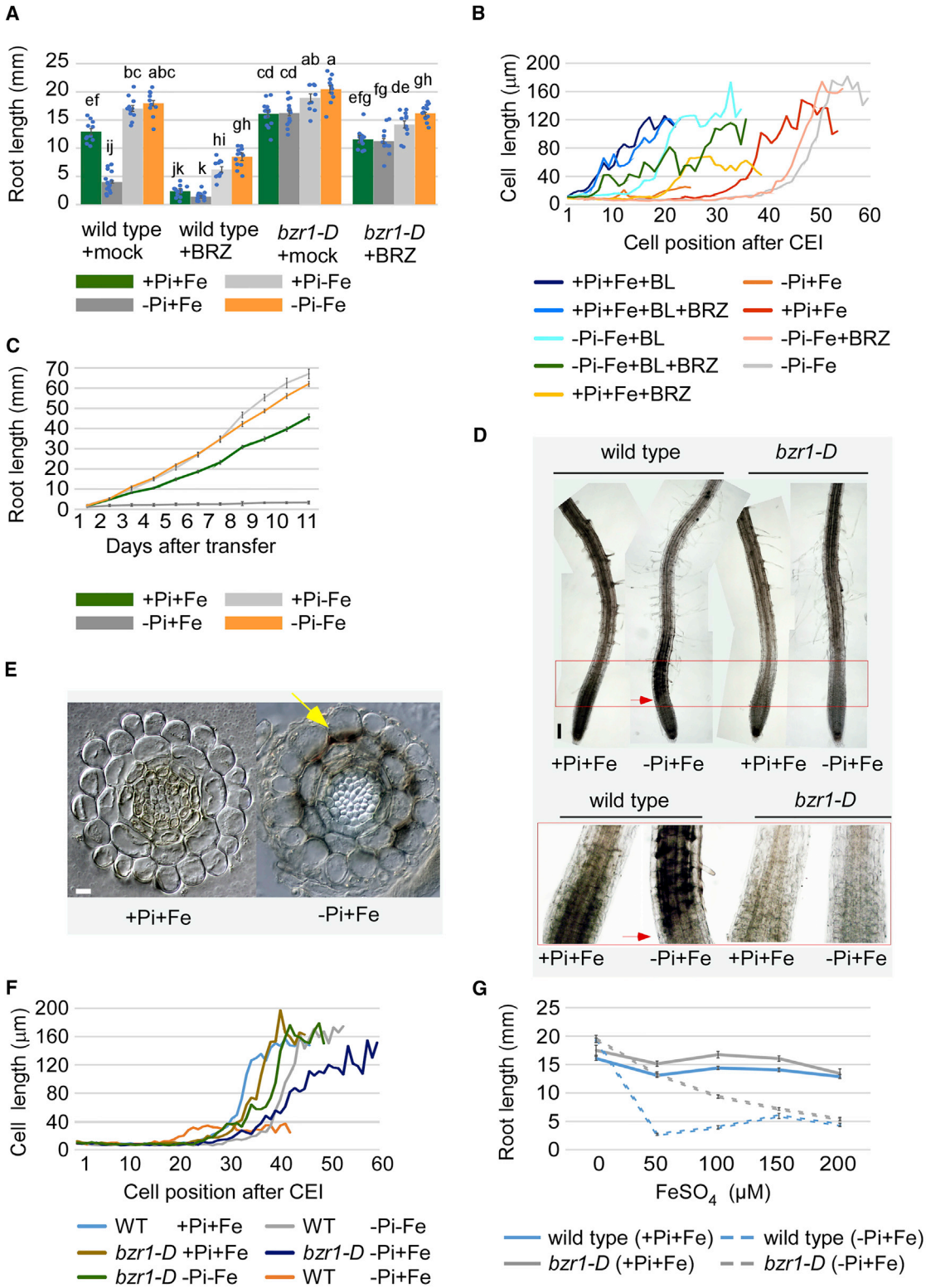

Figure 1. BR Activity Impacts Root Response to Low Pi Conditions by Modulating Fe Accumulation in the Root Elongation Zone

(A) Root length of wild-type and *bzr1-D* plants (n > 20, three biological experiments) grown in the presence or absence (+mock) of the BR biosynthesis inhibitor BRZ, and grown under different combinations of Pi and Fe concentrations. Data are presented as mean ± SEM. The different letters above the columns indicate significant differences between all genotypes and all growth conditions ($p \leq 0.05$).

(legend continued on next page)

et al., 2013; Sun et al., 2013; Belkhadir and Jaillais, 2015). In the cytoplasm, the BRI1/BAK1 complex is inhibited by BRASSINSOSTEROID KINASE INHIBITOR1 (BKI1) (Jaillais et al., 2011; Wang and Chory, 2006), which is associated to the plasma membrane by its membrane hook, controlled by membrane surface charges (Simon et al., 2016), and binds to the BRI1 kinase domain through its C-terminal tail. Upon ligand perception, BRI1 phosphorylates BKI1 and triggers its release from the plasma membrane. This allows further activation of the BRI1/BAK1 complex and of the signaling pathway (Jaillais et al., 2011; Wang and Chory, 2006). A series of additional regulatory steps lead to inhibition of the GSK3-like kinase BRASSINOSTEROID INSENSITIVE2 (BIN2), the key inhibitor of the cascade (Zhu et al., 2017; Kim et al., 2009; Li et al., 2001). Consequently, BRASSINAZOLE RESISTANT1 (BZR1) and BRI1-EMS-SUPPRESSOR1 (BES1)/BZR2 (hereafter called BES1), highly homologous transcription factors, accumulate in the nucleus as de-phosphorylated proteins and regulate gene expression (Yu et al., 2011; Sun et al., 2010). Dominant mutations (bes1-D and bzr1-D) promote a hypophosphorylated state, resulting in their constitutive activity and consequential suppression of different phenotypic abnormalities in BR-insensitive and BR-deficient mutants (Wang et al., 2002; Yin et al., 2002). We have previously demonstrated that constitutive activity of BES1/BZR1 blocks the root response to low Pi availability (Singh et al., 2014). We also showed that low Pi increases the cytoplasm-to-nucleus ratio of BES1/BZR1 (Singh et al., 2014). However, the mechanisms that govern these responses to a limited-nutrient environment remain unknown.

Here, we observed interdependent regulation of Fe-derived signals and BR activity that imparted opposing effects on root growth in response to two nutrient stresses: low Pi (that triggers Fe accumulation in the root) and low Fe. We demonstrate that perturbation of BR signaling components impacted Fe distribution in the root. In turn, the extent of Fe accumulation determined BR activity. Unexpectedly, we found that this interplay required BRI1, independently, or requiring minute levels of its hormone ligand. We show that BKI1 levels served as a crosstalk point between BR- and Fe-dependent signals, as Fe levels impact BKI1's translation. In addition, LPR1 was identified as a target repressed by BES1/BZR1, affecting Fe distribution. This mechanism likely allows roots to switch between distinct morphologies across microenvironments where either Pi or Fe is limited.

RESULTS

BZR1 Blocks Low-Pi-Dependent Fe Accumulation in the Root Elongation Zone

To determine whether the interaction between low-Pi responses and BR-mediated control of root growth depends on Fe, root length following culture in medium with four different combinations of adequate (+) and limited (−) Pi and Fe levels was compared (Figure 1A). Low Pi levels inhibited wild-type root growth, while roots with constitutively active BZR1 (*bzr1-D*) remained unaffected, in agreement with our previous findings (Singh et al., 2014). This was also apparent by considering the average cell length versus position from the stem cell, i.e., from the cortex/endodermis initial (CEI) cell (Figure S1A). *bzr1-D* roots were largely insensitive to the effect of the BR biosynthesis inhibitor brassinazole (BRZ), as expected from the constitutive activity of the protein, and were also insensitive to low Pi levels in the presence of the inhibitor (Figure 1A). Exogenous addition of brassinolide (BL) inhibited root growth both in the presence and absence of BRZ (Figure S1B), and roots of both treatments had few meristematic cells (Figure 1B). Hence, supra-optimal BR levels relieve the inhibitory effect of BRZ on final cell size and overall root length but have additional effects on root growth, beyond the impact of constitutive activity of BZR1. The combined BL and low-Pi treatments had an even more severe effect on the meristem that precluded conductance of cellular analysis. Regardless, BL-treated roots showed a moderate insensitivity to low Pi levels (Figure S1B), which was associated with their larger cell size (Figure S1C).

Root growth inhibition by low Pi was mediated by Fe, as confirmed by the removal of Fe from the medium (Figure 1A). Moreover, under limited Fe conditions, wild-type roots were longer as compared with roots grown in adequate conditions, regardless of the Pi levels tested (Figure 1A) and the enhanced growth persisted throughout the 11-day treatment period (Figure 1C). The growth-promoting effect of low Fe correlated with increased meristematic cell counts and final cell size (Figure 1B). Interestingly, when BR levels were low, as in BRZ-treated root, the enhancement of root growth occurred at a higher fold change as compared with the response of roots to low Fe without perturbation of hormone levels (Figure 1A). Indeed, low Fe suppressed the short cells of BRZ-treated roots, suggesting that the inhibitory activity of low BR is relieved by low Fe (Figure 1B). Supra-optimal levels of BL largely compromised the low-Fe-mediated increase in meristematic cell number in both wild-type and

(B) Average cell length versus position from the cortex/endodermis initial (CEI) cell. Wild-type seedlings grown under different combinations of Pi and Fe concentrations and in the presence or absence of BRZ and/or BL, as in (A).

(C) Root length of wild-type plants, as measured daily 1 to 11 days after transfer to different combinations of Pi and Fe concentrations ($n \geq 10$, three biological experiments).

(D) Perl/DAB staining of roots of wild-type and *bzr1-D* plants, 48 hr after transfer from adequate conditions to low-Pi medium (−P + Fe) or to mock (+P + Fe). Upper panel, stitching of overlapping light microscopy images. Lower panel, magnification of the area marked in the upper panel, with enhanced brightness, to highlight differential staining ($n \geq 8$, five biological experiments). Scale bar, 50 μm. Arrow indicates onset of apoplastic Fe accumulation in the elongation zone.

(E) Root cross-sections of Perl/DAB-stained wild-type roots grown as in (D). Arrow highlights Fe accumulation between epidermal and cortical cells. Scale bar, 10 μm.

(F) Cell length measured as in (B), in wild-type and *bzr1-D*.

(G) Wild-type and *bzr1-D* root response, as measured by root length 4 days after transfer to increasing concentrations of Fe ($FeSO_4$) in adequate and low-Pi conditions. Note that sufficiently high Fe concentrations sensitized *bzr1-D* roots to low Pi. Data are represented as mean ± SEM ($n \geq 15$, three biological experiments. See also Table S6A for statistical analysis).

See also Figure S1.

BRZ-treated roots (Figure S1C). In such cases, the still-long roots of BL-treated seedlings suggest that low Fe might also accelerate the cell production rate (Figure S1B).

Although constitutively active BZR1 counteracts root response to low Pi, no difference in total Fe levels was detected between wild-type and *bzr1-D* roots (Singh et al., 2014). To assess whether the absence of response of *bzr1-D* root to low Pi is associated with differential distribution of Fe as compared with wild-type, roots were stained with Perls/3,3′-Diaminobenzidine (DAB), which identifies *in situ* Fe^{2+} and Fe^{3+} (Roschzttardtz et al., 2009). In response to low Pi, wild-type roots showed a dramatic increase in Fe accumulation in the elongation zone and onset of the differentiation zone within the 48 hr tested (shown as dark patches in Figures 1D and S1D–S1F). Cross-sections show that these patches are apoplastic Fe, as previously identified (Müller et al., 2015); however, under the present conditions, Fe mainly accumulated between the cortex and the epidermis (Figure 1E). Under adequate conditions, Fe was detected in the stele, as previously reported (Roschzttardtz et al., 2013). Under low Pi, high Fe in the elongation zone was accompanied by a reduction of Fe in the mature (shootward) zone of the root, indicative of its redistribution (Figures 1D and S1D–S1F). Fe also accumulated in root hair tips. No apparent increase in Fe levels was noted in the meristem within the tested time frame. Cellular analysis showed reduced meristematic cell count and cell size, while these growth parameters remained unaffected in *bzr1-D* roots (Figure 1F). No differences in overall Fe distribution were noted between *bzr1-D* roots grown under adequate versus low Pi conditions, with the exception of enhanced Fe in root hair tips and uniform spread of Fe in the mature zone of the latter group of roots (Figure S1E). Fe levels in the mature root zone of *bzr1-D* grown with adequate Pi levels were similar to those measured in wild-type roots grown under adequate conditions, suggesting that BZR1 may impinge on Fe redistribution in response to low Pi. Assays testing root sensitivity toward increasing concentrations of Fe in combination with low Pi, demonstrated that *bzr1-D* roots were inhibited at higher Fe levels as compared with wild-type roots, and in accordance, accumulated Fe in the elongation zone (Figures 1G and S1G). Moreover, wild-type roots treated with BRZ accumulated more Fe as compared with mock-treated roots grown under adequate conditions (Figure S1H). Taken together, these results suggest that BZR1 blocks high Fe accumulation in elongating/onset of differentiated cells, thereby preventing Fe and hence low-Pi-mediated inhibition of cell elongation and early differentiation.

BZR1 Controls Fe Accumulation via Transcriptional Regulation of *LPR1*

To reveal how BZR1 controls Fe accumulation, we performed RNA-sequencing (RNA-seq) analysis of wild-type and *bzr1-D* roots grown under adequate conditions for 6 days and then transferred to adequate or low-Pi conditions for 24 hr. This time point corresponds to the early response to low Pi and to the onset of Fe accumulation (Figure S1F). The expression level of approximately 60 genes was upregulated by low Pi, with a striking overlap between wild-type and the mutant root responses (Figure 2A, Table S1). The most significant functional category of these genes was "cellular response to phosphate starvation" in both wild-type and *bzr1-D* roots (5.7×10^{-6} and 4.8×10^{-12}, respectively), confirming effective sensing of nutrient deficiency. To determine whether Fe levels in the medium impact the regulation of these genes, real-time analysis of the well-established low-Pi-responsive genes, *AT4* and *PHT1;4,* was performed (Figure 2B); elevation of their transcript levels in response to low Pi proved independent of Fe levels. As such, we searched for candidate genes that are related to Fe homeostasis and that are differentially regulated in wild-type and mutant roots. The RNA-seq analysis highlighted *LPR1* as a downregulated gene in *bzr1-D* roots, irrespective of phosphate levels in the medium (Figure 2C). To determine where in the root BZR1 impacts the expression of *LPR1*, we produced *pLPR1-GUS* lines (Figure 2D). The GUS reporter was highly expressed in the columella, in accordance with Müller et al. (2015) and Svistoonoff et al. (2007), as well as in the elongation zone, albeit at a lower intensity. Interestingly, low-Pi conditions enhanced reporter expression, primarily in the root elongation zone. The reporter expression in this zone was also low in *bzr1-D* but was not elevated in response to low-Pi conditions (Figure 2D). However, treating *bzr1-D;pLPR1-GUS* seedlings with 100 μM Fe for 48 hr enhanced the expression levels of the reporter gene in the elongation zone/differentiation zones (Figure 2E). When seedlings were grown in the presence of BRZ for 2 days, *pLPR1-GUS* was highly expressed along the wild-type primary root, irrespective of Pi levels (Figure 2E). The reporter was also elevated in *bzr1-D*, but to a lesser extent as compared with wild-type, in agreement with the partial insensitivity of *bzr1-D* roots to BRZ (Figure 2E). Real-time PCR, using roots after tip removal, revealed a similar trend of *LPR1* repression by BZR1, thus further supporting the proposed BZR1-mediated LPR1 regulation in the elongation zone (Figure 2F). The BR target *BR6OX2*, was used as a positive control. Public data search revealed *LPR1* as a target of BZR1 in a chromatin immunoprecipitation experiment (Sun et al., 2010). We then measured the equilibrium-binding constants of recombinant BZR1 (His-tagged-BZR1) and BZR1-D (His-tagged-BZR1-D) to fluorescein-labeled double-stranded DNA (dsDNA) containing two of six putative BES1/BZR1 binding elements (Table S2), i.e., a modified BRRE motif (He et al., 2005) *BRRE-1,254* and *E-box-753* (Figures 2G and S2A, Tables S2–S4). dsDNA corresponding to the DWF4 promoter containing the canonical BRRE was used as a positive control. BZR1 displayed the strongest binding affinity (K_D = 201 ± 31 nM) to the *DWF4* sequence and a slightly lower affinity toward the E-box and the modified BRRE (K_D = 253 ± 70 nM and K_D = 305 ± 45, respectively, Table S3A). dsDNA carrying a mutation in the CGTG consensus sequence of BRRE failed to bind the protein, thus confirming the specificity of the measured interactions. BZR1-D exhibited similar binding affinities (Table S3B).

Since the *lpr1* mutant is insensitive to low Pi and *LPR1* is repressed by BZR1, we reasoned that LPR1 acts downstream to BZR1. To test this hypothesis, we produced transgenic lines with constitutive ubiquitous expression of LPR1 (*pUBQ10-LPR1*) in both wild-type and *bzr1-D* backgrounds. All lines had shorter roots as compared with the non-transformed parental lines (Figures 3A, 3B, S3A, and S3B); however, in response to low Fe, they had longer roots, as seen with the non-transformed plants (Figures S3A and S3B). LPR1 suppressed the insensitivity of *bzr1-D* to low Pi, as manifested by root length inhibition

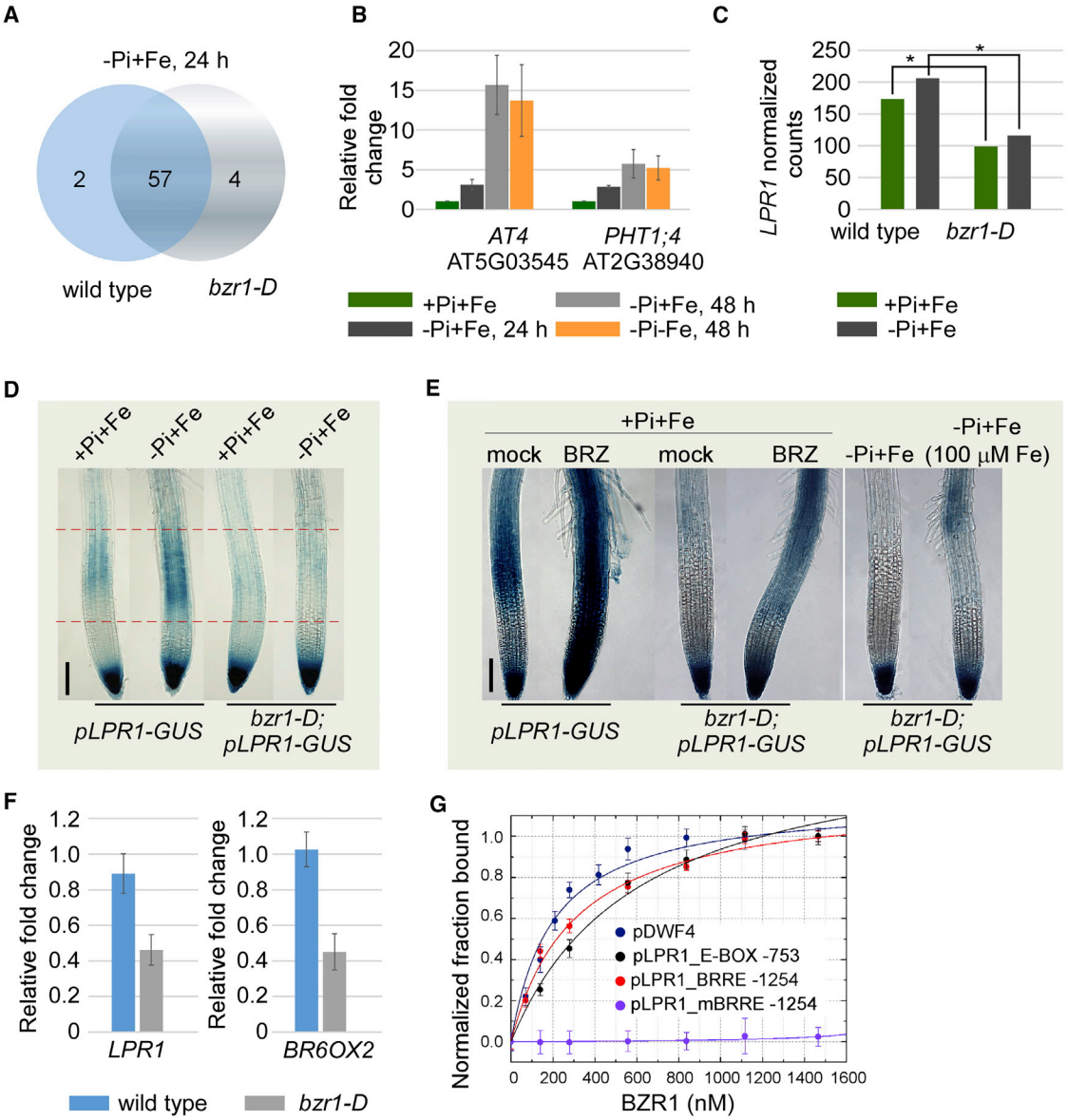

Figure 2. BZR1-D Activity Suppresses *LPR1* Transcription Independent of Pi Availability

(A) Venn diagram showing the number of upregulated genes following a 24-hr exposure to low Pi, in wild-type and *bzr1-D* roots.

(B) Analysis of relative expression of *AT4* and *PHT1;4* following plant growth under adequate conditions, and transfer for 24 hr or 48 hr to −P + Fe or to −P−Fe for 24 hr. Data are presented as mean ± SEM of two biological experiments.

(C) Normalized counts of endogenous *LPR1* transcripts as emerged from the RNA-seq data. The average of two biological replicates is shown. * indicates false discovery rate ≤0.1.

(D and E) GUS reporter analysis of wild-type and *bzr1-D* plants expressing *pLPR1-GUS* grown under adequate conditions for 5 days and then transferred for 48 hr to low Pi, in the absence (D) or presence of BRZ, or to low Pi, supplemented with 100 μM $FeSO_4$ (E). Note that BZR1 primarily suppressed *LPR1* transcript counts in the root elongation zone, unless Fe concentration was elevated in the medium (n > 10, two biological experiments). Scale bar, 100 μm.

(F) Real-time analysis of roots with a detached root meristem, to capture changes in the elongation and differentiation zone in wild-type and *bzr1-D*, in adequate conditions (n = 4 biological repetitions).

(G) Binding of bacterial expressed His-tagged-BZR1 to *pDWRF4*, *pLPR1_E-box-753*, *pLPR1_BBRE −1254* and *pLPR1_mBBRE-1254* dsDNA substrates (30 nM), as measured by fluorescence anisotropy. Solid lines show the best fit of the data. Data are represented as mean ± SEM (n = 3).

See also Figure S2 and Tables S2 and S3.

(Figures 3A, 3B, S3A, and S3B), impaired cell elongation, and hair cell induction (Figures 3C and 3D) in response to decreasing Pi levels. *bzr1-D;pUBQ10-LPR1* roots often displayed a unilateral response to low Pi (Figure 3C), likely arising from their curled morphology and resulting non-uniform contact with the medium. *pUBQ10-LPR1* lines grown under adequate conditions demonstrated high Fe accumulation, in agreement with the observed root growth inhibition (Figure 3D). Fe accumulation along the

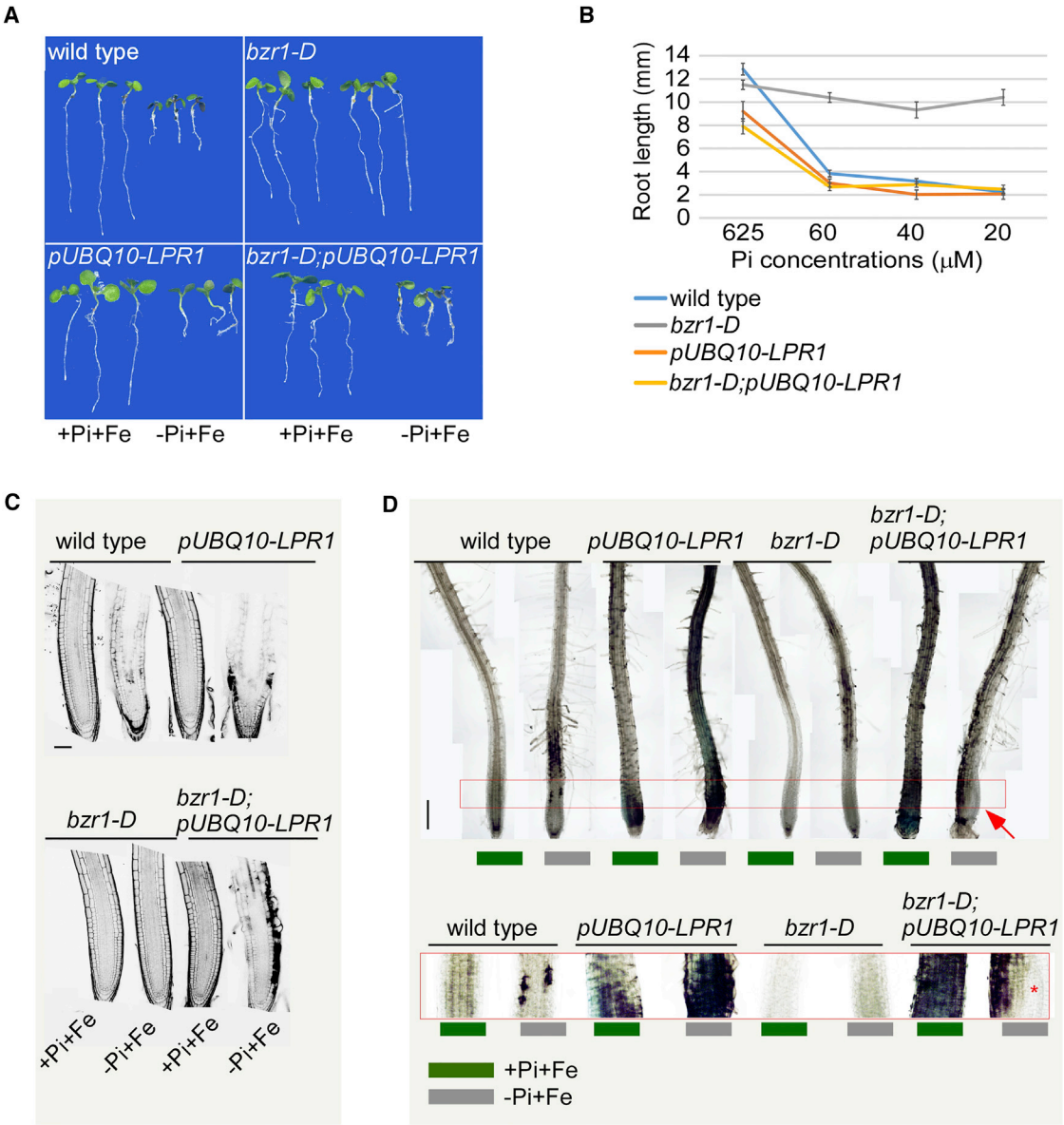

Figure 3. High Expression of LPR1 Suppresses *bzr1-D* Insensitivity to Low Pi by Enhancing Fe Accumulation

(A) Wild-type and *bzr1-D* plants (upper panel) and wild-type and *bzr1-D* plants harboring *pUBQ10-LPR1* (lower panel), grown under adequate or low-Pi conditions for 4 days. Note that high LPR1 expression inhibits *bzr1-D* insensitivity to low Pi.

(B) Root sensitivity to decreasing concentrations of Pi, as measured by root length 4 days after transfer of wild-type and *bzr1-D* plants and of wild-type and *bzr1-D* plants harboring *pUBQ10-LPR1* ($n > 20$, four biological experiments). Data are presented as mean ± SEM. See also Table S6B for statistical analysis.

(C) Confocal microscopy images of seedling of plants presented in (B), grown under adequate conditions with or without transfer to low-Pi conditions for 48 hr ($n \geq 10$, three biological experiments). Scale bar, 50 μm.

(D) Perl/DAB staining in roots of the same genotypes, 48 hr after transfer from adequate conditions to mock (+P+Fe) or to low-Pi medium (−P+Fe). Upper panel, stitching overlapping light microscopy images. Lower panel, magnification of the root elongation zone (area boxed in red in upper panel) to highlight differential staining. Asterisk/arrow, root side that was not in contact with the media. Scale bar, 100 μm ($n \geq 15$, three biological experiments). Note that high LPR1 expression also enhanced Fe accumulation in *bzr1-D*. See also Figure S3.

root, including in the elongation zone, was considerably enhanced in response to low Pi conditions, and corresponded to the severity of the root phenotype. The change in Fe distribution appeared similar in wild-type and *bzr1-D*, suggesting that *bzr1-D* is no longer sensitive to low Pi due to constitutive LPR1-mediated high accumulation of Fe.

Low Fe Promotes Root Growth by Stimulating the BR Pathway Despite Negligible Levels of Hormone Ligand

While low-Pi-mediated high accumulation of Fe in the root elongation zone inhibited root growth, low Fe had a promoting effect, with a higher relative impact on seedlings grown in the presence of BRZ (Figures 1A–1C, 4A, and 4C). By day 15, length

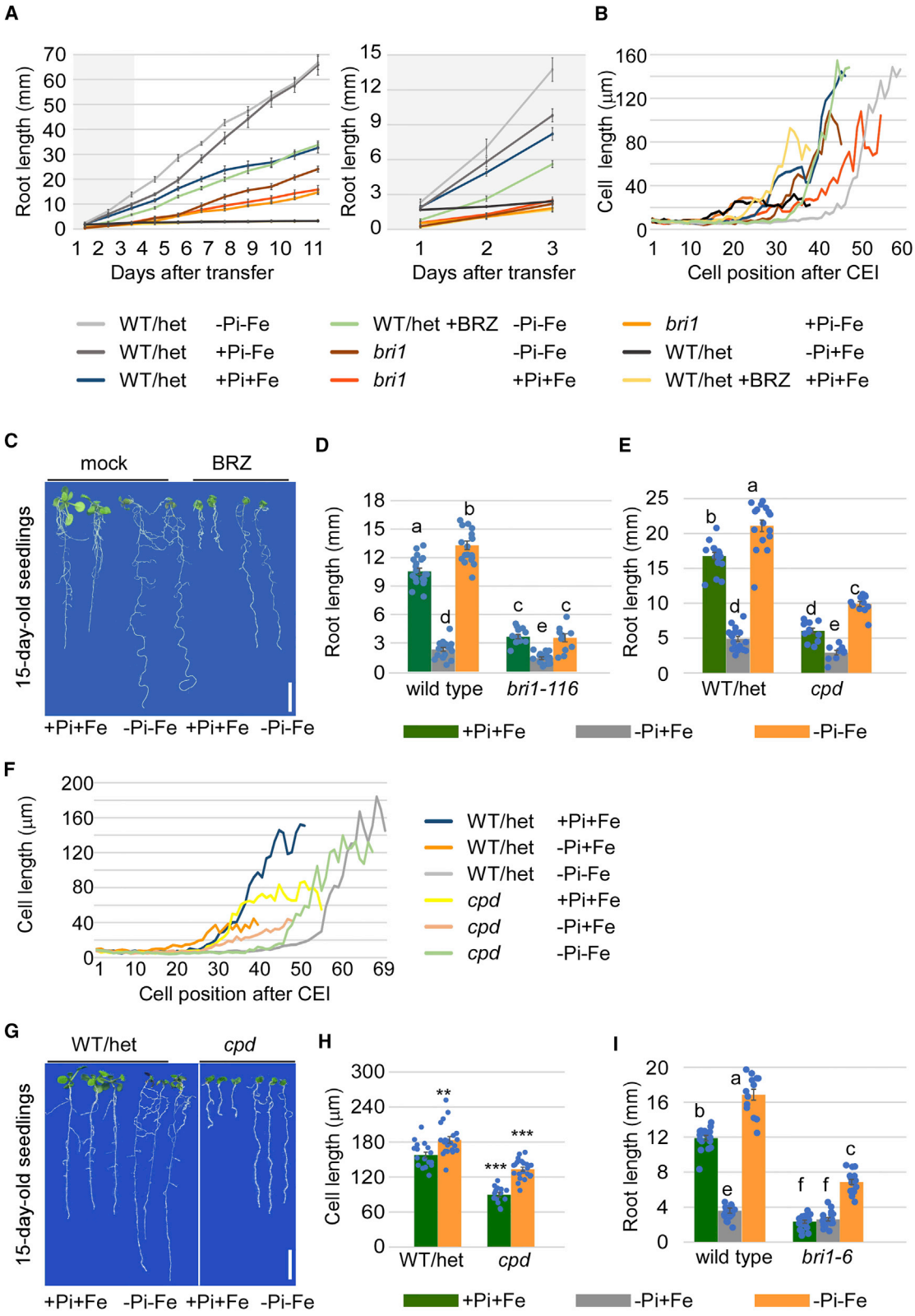

Figure 4. Low Fe Promotes Root Growth Independently of the BR Hormone Ligand

(A) Root length of segregating a *BRI1/bri1* heterozygous population of the null *bri1* allele (GABI_134E10). Seedlings were grown for 4 days in adequate conditions before transfer to different combinations of Pi and Fe concentrations, in the presence or absence of BRZ. Right panel, measurements of the first 3 days after transfer are highlighted. Note that low Fe stimulated root elongation in BRZ-treated plants but not in *bri1*. Data are presented as mean ± SEM.

(legend continued on next page)

of BRZ-treated roots grown in the presence of low Fe was similar to that of wild-type roots grown under adequate conditions (Figures 4B and 4C). Interestingly, low Fe did not promote root growth of null *bri1* alleles within 4 days after transfer (Figures 4A and 4D). Thus, BRI1 is essential for root elongation in early response to low iron availability. Similar to the effect of BRZ, roots of the null and severe BR biosynthesis mutant *cpd* showed a more substantial response to low Fe as compared with those of the parental segregating genetic background, manifested by enhanced growth (Figures 4E–4G) and longer cells (Figures 4F–4H). Under adequate conditions, *bri1-6* plants, harboring the G644D mutation, which is thought to reduce ligand binding to the receptor (Hothorn et al., 2011; Noguchi et al., 1999), had a short root similar to roots with the null *bri1* allele (Figure 4I). However, in response to low Fe conditions, its root displayed enhanced growth (about 3-fold) as compared with adequate conditions (Figure 4I). No change in BR biosynthesis genes was detected in roots within 24 hr of root exposure to low Pi (Figure S2B). Taken together, these observations suggest that low Fe levels induce root growth via BRI1, either in a ligand-independent manner or requiring negligible levels.

BKI1 Accumulation: A Crosstalk Point between BR- and Fe-Dependent Signals

We next addressed the hypothesis that low Fe triggers BR signaling at the plasma membrane by relieving an inhibitory component. High BKI1 levels, as in 35S-BKI1, inhibit the BR signaling pathway (Wang and Chory, 2006), while the null *bki1-1* mutant exhibits partially activated BR signaling (Jiang et al., 2015). To assess whether BKI1 is modulated by low-Pi-mediated Fe availability, both *35S-BKI1-YFP* and *pUBQ10-BKI1-mCHERRY* lines were monitored after exposure to adequate (+P+Fe, 48 hr) versus inadequate (−P+Fe, 24 hr or 48 hr, followed by −P−Fe for 24 hr) conditions (Figures 5A–5D, S4A, S4B, and S4E). Higher accumulation of BKI1 was observed in seedlings exposed to −P+Fe as compared with adequate conditions, mainly in the root elongation zone (Figures 5A–5D). This elevation appeared higher in *pUBQ10-BKI1-mCHERRY* as compared with *35S-BKI1-YFP*, reminiscent of a previously reported differential response of the two protein fusions (Jaillais et al., 2011). In contrast, within 24 hr of transfer to −P−Fe, BKI1 levels were lower as compared with samples grown under adequate conditions (Figures 5B, 5D, and S4A–S4C). This reduction consistently appeared in the onset of cell elongation and occasionally in the meristem. In agreement, no iron accumulated in the root elongation zone when seedling transfer to −P−Fe for 24 hr after 24 hr on low Pi (Figure S4H). Seedling transfer to −P−Fe for 24 hr after 24 hr or 48 hr on low Pi, resulted in lower levels of BKI1, including in BRZ-treated roots (Figures S4C and S4D). Thus, Pi-mediated Fe levels control BKI1 accumulation within the tested 24-hr time frame, irrespective of BR levels. We next asked whether the differential accumulation of BKI1 is a result of differential stability of the protein. To this end, we established transgenic lines expressing *BKI1-mCitrine* under the heat shock inducible promoter and quantified the protein levels in the plasma membrane and cytoplasm after heat shock (Figures 5E, 5F, S4F, and S4G). BKI1 reached higher levels in −P+Fe conditions and lower levels in −P−Fe as compared with adequate conditions (Figure 5F). However, protein decay was independent of Fe levels (Figure 5G). Across tested conditions, the density of BKI1 at the plasma membrane was higher as compared with the cytoplasm, and this ratio only slightly varied over time (Figures S4F and S4G). Together, the absolute high and the low BKI1 levels at the plasma membrane in −P+Fe and −Pi−Fe, respectively, as also observed after heat shock, are unlikely due to regulation of its stability. Therefore, we hypothesized that BKI1 is translated at different efficiencies and, hence, compared BKI1 transcript levels in total RNA and in association with polyribosomes, using a transgenic line expressing 35S:HF-RPL18 (Vragovic et al., 2015; Zanetti et al., 2005) (Figure 5H). BKI1 transcript was more frequently associated with RPL18 in roots subjected to −P+Fe conditions, while the level of free transcript remained largely unchanged. This suggests that the translation efficiency of BKI1 is enhanced under these conditions. Next, we set out to determine the relevance of BKI1 levels in root response to low Pi. The null *bki1-1* mutant showed reduced sensitivity to low Pi as compared with wild-type (Figure 5I). In response to moderate Pi doses (60 μM), *bki1-1* showed insensitivity similar to *lpr1*, which was gradually decreased with the drop in the Pi concentration. *bzr1-D* was fully insensitive to all Pi concentrations tested. In addition, *35S-BKI1-YFP* had higher basal Fe levels as compared with wild-type (Figure S4I). Taken together, low Pi/Fe levels appear to control BKI1 accumulation via translation efficiency that, in turn, impinges on Fe accumulation and subsequently on root response to low Pi. Thus, changes in BKI1 levels influence, at least in part, the BRI1-dependent effect of iron.

Fe and LPR1 Impact BES1/BZR1 Activity

Low-Pi-mediated Fe accumulation and low Fe levels inhibit and activate the BR pathway, respectively. As such, it is expected that BES1/BZR1 will be modulated within the same time frame

(B) Average cell length versus position from CEI, in lines and conditions as in (A).
(C) Seedlings grown for 4 days before transfer to mock (adequate conditions) or to −P−Fe, in the presence or absence of BRZ, respectively, for an additional 11 days (i.e., 15-day-old seedlings, n ≥ 15, three biological experiments). Scale bar, 1 cm.
(D) Root length of wild-type or *bri1-116* (null mutant) 8-day-old seedlings. Seedlings were grown under adequate conditions for 4 days before transfer for an additional 4 days to low-Pi medium, with or without Fe (−P+Fe and −P−Fe, respectively) or to mock conditions (i.e., adequate conditions, +P+Fe). Data are presented as mean ± SEM. The different letters indicate significant differences between all genotypes and all growth conditions ($p \leq 0.05$) (n ≥ 12, three biological experiments).
(E) Root length of segregating *CPD/cpd* heterozygous population, grown as in (D). Data are presented as mean ± SEM (n ≥ 13, four biological experiments).
(F) Average cell length versus position from CEI in genotypes and conditions as in (E).
(G) Plants of the same genotypes as in (E), 11 days after transfer to low Pi and low Fe (−P−Fe) or to adequate (+P+Fe) conditions. Scale bar, 1 cm.
(H) Final cortical cell length of segregating *CPD/cpd* plants grown as in (D). A comparison between adequate conditions and low Pi and low Fe is shown (n ≥ 10, three biological experiments). Data are presented as mean ± SEM. **$p < 0.01$; ***$p < 0.001$ with two-tailed Student's t test.
(I) Root length of *bri1-6* (mutant with impaired ligand binding) grown as in (D). Data are presented as mean ± SEM (n ≥ 18, two biological experiments).

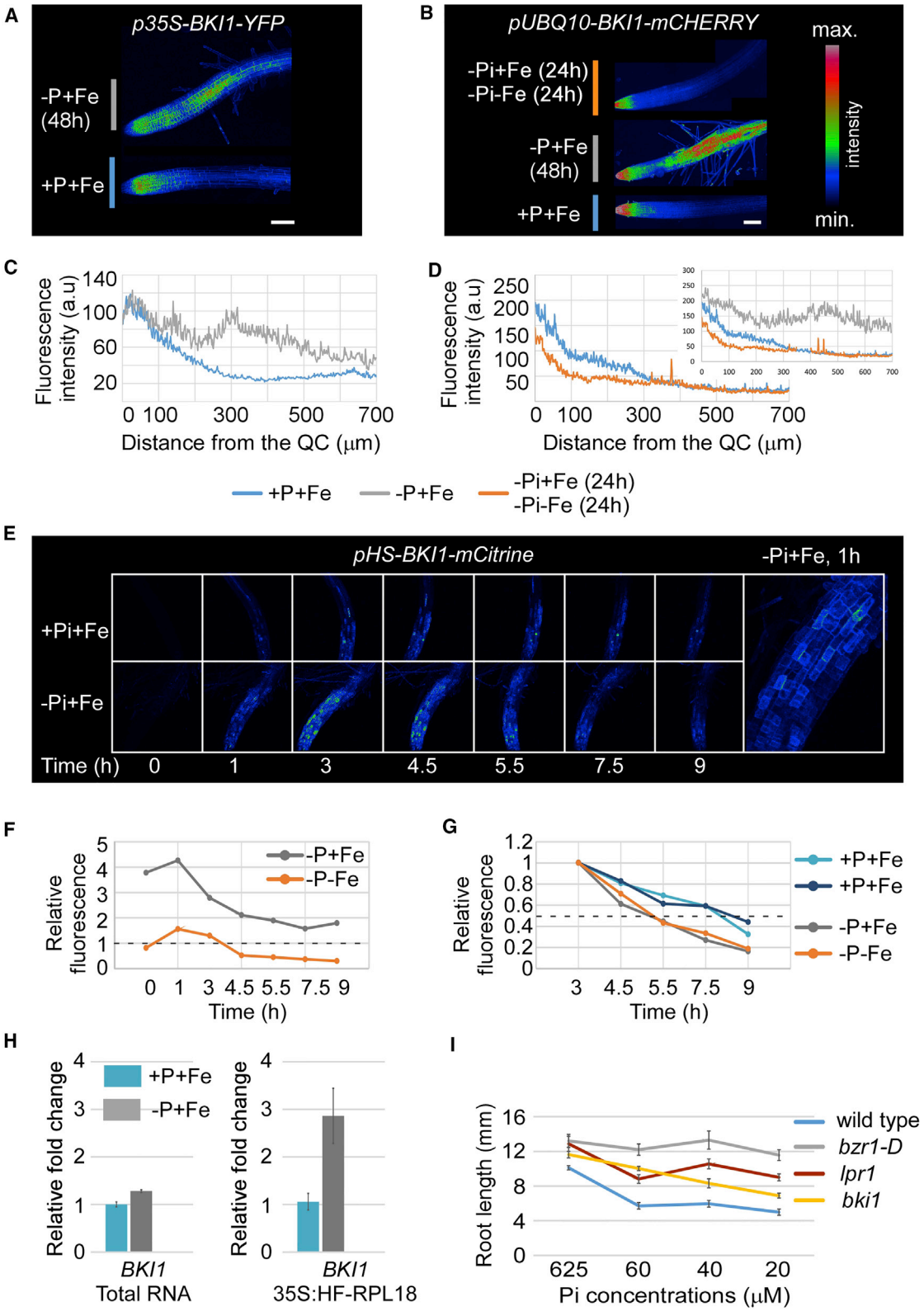

Figure 5. BKI1 Is Modulated by Low-Pi-Mediated Fe Accumulation

(A and B) (A) BKI1-YFP and (B) BKI1-mCHERRY signals after plant transfer to different nutrient availability conditions, as indicated. Maximal projection images are shown. Confocal images are color-coded with respect to pixel intensity based on the scale shown. Scale bar, 100 μm.

(legend continued on next page)

as BKI1. Indeed, an increase in the phosphorylated (i.e., inactive) form of BES1 was detected within 24 hr of exposure to low Pi (Figure 6A), while low Fe (−P−Fe) favored the de-phosphorylated (i.e., active) form within 24 hr, thus providing independent molecular evidence for the inhibition and activation of the BR signaling pathway by Pi/Fe availability. Quantification of the ratio between phosphorylated and de-phosphorylated BES1 lay in line with this trend, with low Fe, in the presence or absence of BRZ, reducing this ratio as compared with adequate conditions (Figure 6A, lower panel, Figure 6B). BR treatment served as a positive control, and yielded the highest reduction in the inactive-to-active ratio. Finally, within 24 hr of transfer to −Pi−Fe, BZR1 and BES1 accumulated in the nucleus, considerably altering the low Pi-mediated high cytoplasmic-to-nuclear ratio (Figures 6C and 6D) (Singh et al., 2014). Moreover, low Fe enhanced the accumulation of BZR1 in the nucleus as compared with adequate conditions, thereby supporting the suggested low-Fe-mediated activation of BES1/BZR1 (Figure 6C). A similar trend was also noted when *BES1* was expressed under the pUBQ10 promoter (Figure 6D). In agreement with low-Fe-mediated activation of BES1/BZR1, the *pLPR1-GUS* reporter level was reduced within 48 hr of transfer to low Fe, regardless of BRZ treatment (Figure S5). Since LPR1 levels impact Fe distribution, we asked whether gain- and loss-of-function of *LPR1* would also modulate BR activity. *lpr1* proved hyposensitive to BRZ-induced reductions in BR levels, similar to *bki1-1* (Figure 6E). In agreement, *pUBQ10-LPR1* lines showed increased sensitivity to BRZ (Figure 6F). Hence, Fe levels impact BR activity and, in turn, BR activity controls Fe accumulation.

DISCUSSION

BR Activity in the Root Is Modulated by Nutrient Composition and Vice Versa

This study uncovered the reciprocal control of nutrient and hormonal signals as a means to achieve growth plasticity (Figure 6G). This was demonstrated by the concomitant perturbation of Fe accumulation and BR activity in the presence of gain- and loss-of-function mutations in LPR1 and BR signaling components (e.g., BKI1). In addition, the overlapping spatial distribution and dynamics of components shared between BR and Fe signals were evidence of the tight interplay between the two pathways. More specifically, BKI1 levels were modulated primarily in the elongation zone and in the onset of the differentiation zones, where low Pi mediates Fe accumulation. In parallel, LPR1 modulation by BES1/BZR1 occurred primarily in this zone. This study demonstrated that the accumulation of BKI1 (and inherently, the activity of BES1/BZR1) is also shaped by the environment, independently of BR levels. Specifically, low-Pi-mediated Fe accumulation enhanced BKI1 levels by affecting its translation efficiency. Interestingly, long-term exposure to low Pi has been recently reported to affect the translation efficiency of selected genes (Bazin et al., 2017). How this is achieved is an intriguing subject for future studies. Low Fe yielded lower levels of BKI1, and higher BES1/BZR1 activity, even under low BR levels. Hence, BRI1 likely has a basal activity that is otherwise blocked by BKI1. This is evident by the longer *bki1* root in the presence of BRZ as compared with wild-type. Taken together, the expression pattern and activation of BR components in the root, and the resulting extent of growth, is an outcome of linked hormonal distribution and nutrient status.

Root Cell Elongation as a Target of Opposing BR and Fe Signals

In agreement with the site of BR/Fe spatial modulation, BR activity and Fe signals were shown here to have opposite effects on cell elongation. For example, adequately high levels of LPR1 suppressed *bzr1-D* and its insensitivity to low Pi. Likewise, when LPR1 was expressed at normal levels, *bzr1-D* became insensitive to low Pi, and maintained elongated cells. Low-Pi-mediated Fe also triggered loss of meristem via LPR1 (Gutierrez-Alanis et al., 2017; Müller et al., 2015) and in agreement, BZR1 activity prevented this effect. In the apoplast, high Fe triggers accumulation of reactive oxygen species, which is accompanied by cell wall stiffening and inhibition of cell elongation (Balzergue et al., 2017; Hoehenwarter et al., 2016; Müller et al., 2015). Our data showed that low Fe triggers root elongation by enhancing the size of the meristem and the final cell size, plausibly through reduced stiffness of the cell wall. This is supported by the reported role of BR activity in controlling cell wall deposition and final cell size in the epidermis (Fridman et al., 2014). Indeed, Fe accumulation was highest in the apoplast surrounding these cells. In agreement with the mutual effect of Fe and BR, *lpr1* is insensitive to BRZ to the same extent as *bki1-1*. In the absence (or presence of minute levels) of the hormone ligand, low Fe triggered root growth more effectively than the LPR1 and BKI1 loss-of-function mutations, likely due to gene redundancy (e.g., *lpr1lpr2* was more insensitive to low Pi as compared with the

(C and D) Quantification of the fluorescence signal as a function of distance from the QC of roots in (A) and (B), respectively. The smaller graph in (D) also includes BKI1 signal in low Pi. Note that high BKI1 signals were triggered by low Pi at the onset of elongation and differentiation zones, an elevation that was relieved by low Fe within 24 hr.

(E and F) Time series of BKI1 fluorescence signal after heat shock, applied 48 hr after transfer from +P+Fe to −P+Fe or −P−Fe. (E) Shown is an example of confocal images corresponding to two roots expressing *pHS-BKI1-mCitrine* that were heat-shocked after transfer to adequate or to −P+Fe at the indicated time. One image is enlarged for clarity. Confocal images are color-coded as in (A). (F) Quantification of fluorescence signal of BKI1-mCitrine after heat shock applied 48 hr after transfer from +P+Fe to −P+Fe or −P−Fe. Signal at the plasma membrane in −P+Fe or −P−Fe, relative to adequate conditions (+P+Fe), is shown (five to six roots per condition, eight to ten cells per root).

(G) Decay of the BKI1-mCitrine signal at the plasma membrane relative to its maximal intensity measured 3 hr after heat shock in −P+Fe, −P−Fe and their corresponding adequate condition controls. Dashed line indicates half-life of the protein.

(H) Real-time analysis of *BKI1* transcript in roots, 48 hr after transfer to −P+Fe. Relative levels in total RNA and after association with ribosomal protein, as a proxy to translation, are shown (n = 3 biological repetitions).

(I) Wild-type, *bzr1-D*, *lpr1,* and *bki1-1* root sensitivity to decreasing concentrations of Pi, as measured by root length. Data are presented as mean ± SEM ($n \geq 15$, three biological experiments, see Supplemental Information text for statistical analysis).

See also Figure S4.

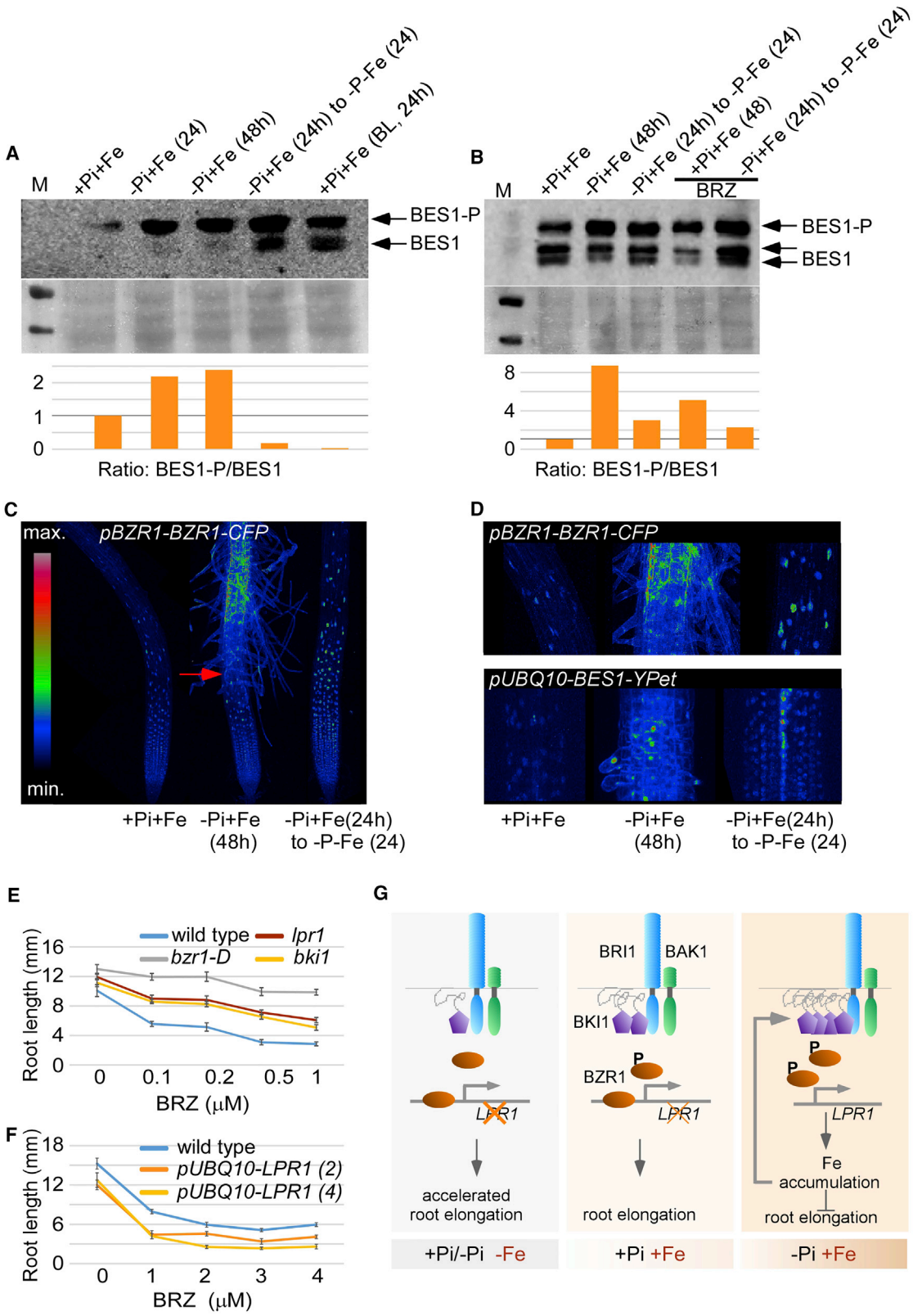

Figure 6. Fe Availability Regulates BR Signaling

(A) Western blot analysis of protein extracted from wild-type roots, analyzed by antibodies against endogenous BES1. Seedlings were grown under adequate conditions before transfer to different nutrient availability conditions, as indicated and for the indicated durations. Treatment with the BR hormone (BL, 50 nM) was

(legend continued on next page)

single mutants). Alternatively, BRI1 is regulated by Fe via additional unknown factors. In accordance with the minor contribution of the ligand to the effect of Fe, no change in BR biosynthesis genes was detected within this time frame of exposure to low Pi. However, long-term exposure to low Pi (7 days) reduced the expression of these genes (Singh et al., 2014). Moreover, root growth of *bri1* was stimulated after 5 days of exposure to low Fe. Hence, the nutrient status likely imparts multi-layered, time-sensitive regulation on root growth. In this model, the early response involves a BRI1-dependent effect, whereas long-term response involves changes in other pathways.

Significance of Interwoven BR and Pi/Fe Signals

In accordance with the heterogeneous characteristic of the soil, Fe and Pi availability vary in different microenvironments. When Pi is limited, interwoven Fe/low-BR signals may drive Fe-dependent morphological changes, i.e., increased lateral root density. Under these conditions, roots also secrete acid phosphatases to the rhizosphere, thereby boosting Pi scavenging and mobilization from insoluble compounds. When Pi is limited, the presence of apoplastic Fe could also serve as a protective mechanism to prevent Fe entry into the cell. In case of limited Fe availability, plants, with the exception of grasses, acquire Fe by increasing proton efflux, followed by Fe reduction and transport on the cell membrane (Marschner and Romheld, 1994) (Thomine and Vert, 2013). While the biochemical events on the plasma membrane are important, the impact of potentially secreted Fe chelates is limited. As such, the plant may benefit from continuous foraging of the soil, facilitated by low Fe linked to high BR activity in elongating cells, which promote root growth. Fe concentrations have a different impact on hormonal responses. High local Fe induces lateral root elongation via auxin (Giehl et al., 2012), whereas severe Fe deprivation inhibits primary root growth by promoting the accumulation of the gibberellin inhibitor DELLA in the root meristem and the root elongation zone (Wild et al., 2016). Intriguingly, low Pi triggering high Fe accumulation had a similar effect on DELLA in these same root zones (Jiang et al., 2007). How plants distinguish between severe and mild Fe deficiency stress remains to be determined.

In summary, this work highlights root growth plasticity as dictated by nutrient availability. A feedback between Fe and BR, that reciprocally impacts their signaling strength and thereby dictates a flexible growth response, is presented. This mechanism is expected to facilitate plant adaptation to distinct microenvironments in the soil. As such, it would be interesting to explore the universality of this strategy across plant species and in different habitats.

STAR★METHODS

Detailed methods are provided in the online version of this paper and include the following:

- KEY RESOURCES TABLE
- CONTACT FOR REAGENT AND RESOURCE SHARING
- EXPERIMENTAL MODEL AND SUBJECT DETAILS
  - Plant Material, Growth Conditions and Treatments
- METHOD DETAILS
  - RNA Extraction and Expression Analysis
  - Histochemical Detection and Light Microscopy
  - Protein Extraction and Western Blotting
  - DNA Binding Measurements by Fluorescence Anisotropy
  - Live Imaging and Confocal Microscopy
  - Heat Shock of *pHS-BKI1-mCitrine*
  - Constructs and Transgenic Lines
- QUANTIFICATION AND STATISTICAL ANALYSIS
  - Sequencing and Data Analysis
  - Analysis of Physiological Measurements
- DATA AND SOFTWARE AVAILABILITY

SUPPLEMENTAL INFORMATION

Supplemental Information includes five figures and six tables and can be found with this article online at https://doi.org/10.1016/j.devcel.2018.06.002.

ACKNOWLEDGMENTS

We thank M. Shenker (HUJI) and A. Eshel (TAU) for the fruitful discussions. We also thank Y. Yin (ISU) for providing anti-BES1 antibodies; T. Asami (UTokyo) for providing BRZ; J. Li (UM-Peking University and UMS), M. Szekeres (BRC), B. Poppenberger (TUM), Z. Wang (Stanford), and X. Wang (Huazhong Agricultural University) for sharing published material; the NASC collection for providing transgenic *Arabidopsis* lines; and R. Fluhr, B. Horwitz, and members of the lab for their critical review of the paper. We are grateful to Ayelet Kurtz and Dan Eisler for their technical assistance, to Smadar Goldstein for the graphical abstract, to the Life Sciences and Engineering Infrastructure Center and Russell Barrie Nanotechnology Institute at the Technion. A.P.S. was supported by the PBC Fellowship Program for Outstanding Post-doctoral Fellows from China and India 2012/2013. This research was supported by grants from ERC no. 3363360-APPL under FP/2007–2013 to Y.J., Israel Science Foundation (296/13) to A.H., and the United States-Israel Binational Agricultural Research and Development Fund (IS-BARD IS-4827-15), Israel Science Foundation (2649/16), and Fund for Applied Research at the Technion to S.S.-G.

AUTHOR CONTRIBUTIONS

Conceptualization, A.P.S. and S.S.-G.; Investigation, A.P.S., Y.F., N.H., M.A.-L., R.Z., and A.H.; Resources, Y.J.; Writing, A.P.S. and S.S.-G.

used as a control for enrichment of de-phosphorylated BES1. Middle panel shows Ponceau staining to demonstrate total protein levels in the corresponding samples. Lower panel shows the ratio of phosphorylated (BES1-P) to de-phosphorylated (BES1) forms of BES1. This ratio in adequate conditions was set to 1 and the ratio in the other samples were normalized, accordingly.

(B) Western blot analysis as in (A), but in the absence or presence of BRZ.

(C) *pBZR1-BZR1-CFP* after transfer to different nutrient availability conditions, as indicated and for the indicated durations. Maximal projection images are shown. The red arrow marks the onset of high cytoplasmic accumulation of BZR1.

(D) Upper panel, magnification of the elongation/differentiation zone as in (C). Lower panel, *pUBQ10-BES1-YPet* grown as in (C).

(E) Root length of wild-type, *bzr1-D*, *lpr1*, and *bki1* plants in the presence of increasing concentrations of BRZ ($n \geq 15$, three biological experiments).

(F) Root length of wild-type and two independent *pUBQ10-LPR1* lines in the presence of increasing concentrations of BRZ. Data are presented as mean ± SEM. See Tables S6C and S6D for statistical analysis ($n \geq 15$, two biological experiments).

(G) Model for interdependent control of nutrient and steroid signals.

DECLARATION OF INTERESTS

The authors declare no competing interests.

Received: March 6, 2017
Revised: March 27, 2018
Accepted: June 4, 2018
Published: July 2, 2018

REFERENCES

Asami, T., Min, Y.K., Nagata, N., Yamagishi, K., Takatsuto, S., Fujioka, S., Murofushi, N., Yamaguchi, I., and Yoshida, S. (2000). Characterization of brassinazole, a triazole-type brassinosteroid biosynthesis inhibitor. Plant Physiol. *123*, 93–100.

Balzergue, C., Dartevelle, T., Godon, C., Laugier, E., Meisrimler, C., Teulon, J.M., Creff, A., Bissler, M., Brouchoud, C., Hagege, A., et al. (2017). Low phosphate activates STOP1-ALMT1 to rapidly inhibit root cell elongation. Nat. Commun. *8*, 15300.

Bazin, J., Baerenfaller, K., Gosai, S.J., Gregory, B.D., Crespi, M., and Bailey-Serres, J. (2017). Global analysis of ribosome-associated noncoding RNAs unveils new modes of translational regulation. Proc. Natl. Acad. Sci. USA *114*, E10018–E10027.

Belkhadir, Y., and Jaillais, Y. (2015). The molecular circuitry of brassinosteroid signaling. New Phytol. *206*, 522–540.

Dong, J., Pineros, M.A., Li, X., Yang, H., Liu, Y., Murphy, A.S., Kochian, L.V., and Liu, D. (2017). An *Arabidopsis* ABC transporter mediates phosphate deficiency-induced remodeling of root architecture by modulating iron homeostasis in roots. Mol. Plant *10*, 244–259.

Fridman, Y., Elkouby, L., Holland, N., Vragovic, K., Elbaum, R., and Savaldi-Goldstein, S. (2014). Root growth is modulated by differential hormonal sensitivity in neighboring cells. Genes Dev. *28*, 912–920.

Fridman, Y., Holland, N., Elbaum, R., and Savaldi-Goldstein, S. (2016). High resolution quantification of crystalline cellulose accumulation in *Arabidopsis* roots to monitor tissue-specific cell wall modifications. J. Vis. Exp. https://doi.org/10.3791/53707.

Giehl, R.F., Lima, J.E., and von Wiren, N. (2012). Localized iron supply triggers lateral root elongation in *Arabidopsis* by altering the AUX1-mediated auxin distribution. Plant Cell *24*, 33–49.

Gonzalez-Garcia, M.P., Vilarrasa-Blasi, J., Zhiponova, M., Divol, F., Mora-Garcia, S., Russinova, E., and Caño-Delgado, A.I. (2011). Brassinosteroids control meristem size by promoting cell cycle progression in *Arabidopsis* roots. Development *138*, 849–859.

Gruber, B.D., Giehl, R.F., Friedel, S., and von Wiren, N. (2013). Plasticity of the *Arabidopsis* root system under nutrient deficiencies. Plant Physiol. *163*, 161–179.

Gutierrez-Alanis, D., Yong-Villalobos, L., Jimenez-Sandoval, P., Alatorre-Cobos, F., Oropeza-Aburto, A., Mora-Macias, J., Sanchez-Rodriguez, F., Cruz-Ramirez, A., and Herrera-Estrella, L. (2017). Phosphate starvation-dependent iron mobilization induces CLE14 expression to trigger root Meristem differentiation through CLV2/PEPR2 signaling. Dev. Cell *41*, 555–570.

Hacham, Y., Holland, N., Butterfield, C., Ubeda-Tomas, S., Bennett, M.J., Chory, J., and Savaldi-Goldstein, S. (2011). Brassinosteroid perception in the epidermis controls root meristem size. Development *138*, 839–848.

Hanlon, M.T., Ray, S., Saengwilai, P., Luthe, D., Lynch, J.P., and Brown, K.M. (2018). Buffered delivery of phosphate to *Arabidopsis* alters responses to low phosphate. J. Exp. Bot. *69*, 1207–1219.

He, J.X., Gendron, J.M., Sun, Y., Gampala, S.S., Gendron, N., Sun, C.Q., and Wang, Z.Y. (2005). BZR1 is a transcriptional repressor with dual roles in brassinosteroid homeostasis and growth responses. Science *307*, 1634–1638.

Hoehenwarter, W., Monchgesang, S., Neumann, S., Majovsky, P., Abel, S., and Muller, J. (2016). Comparative expression profiling reveals a role of the root apoplast in local phosphate response. BMC Plant Biol. *16*, 106.

Hothorn, M., Belkhadir, Y., Dreux, M., Dabi, T., Noel, J.P., Wilson, I.A., and Chory, J. (2011). Structural basis of steroid hormone perception by the receptor kinase BRI1. Nature *474*, 467–471.

Jaillais, Y., Hothorn, M., Belkhadir, Y., Dabi, T., Nimchuk, Z.L., Meyerowitz, E.M., and Chory, J. (2011). Tyrosine phosphorylation controls brassinosteroid receptor activation by triggering membrane release of its kinase inhibitor. Genes Dev. *25*, 232–237.

Jiang, C., Gao, X., Liao, L., Harberd, N.P., and Fu, X. (2007). Phosphate starvation root architecture and anthocyanin accumulation responses are modulated by the gibberellin-DELLA signaling pathway in *Arabidopsis*. Plant Physiol. *145*, 1460–1470.

Jiang, J.J., Wang, T., Wu, Z.H., Wang, J., Zhang, C., Wang, H.J., Wang, Z.X., and Wang, X.L. (2015). The intrinsically disordered protein BKI1 is essential for inhibiting BRI1 signaling in plants. Mol. Plant *8*, 1675–1678.

Karimi, M., Depicker, A., and Hilson, P. (2007). Recombinational cloning with plant gateway vectors. Plant Physiol. *145*, 1144–1154.

Kim, T.W., Guan, S., Sun, Y., Deng, Z., Tang, W., Shang, J.X., Sun, Y., Burlingame, A.L., and Wang, Z.Y. (2009). Brassinosteroid signal transduction from cell-surface receptor kinases to nuclear transcription factors. Nat. Cell Biol. *11*, 1254–1262.

Li, J., and Chory, J. (1997). A putative leucine-rich repeat receptor kinase involved in brassinosteroid signal transduction. Cell *90*, 929–938.

Li, J., Nam, K.H., Vafeados, D., and Chory, J. (2001). BIN2, a new brassinosteroid-insensitive locus in *Arabidopsis*. Plant Physiol. *127*, 14–22.

Lynch, J. (1995). Root architecture and plant productivity. Plant Physiol. *109*, 7–13.

Lynch, J.P. (2011). Root phenes for enhanced soil exploration and phosphorus acquisition: tools for future crops. Plant Physiol. *156*, 1041–1049.

Marques-Bueno, M.D.M., Morao, A.K., Cayrel, A., Platre, M.P., Barberon, M., Caillieux, E., Colot, V., Jaillais, Y., Roudier, F., and Vert, G. (2016). A versatile Multisite Gateway-compatible promoter and transgenic line collection for cell type-specific functional genomics in *Arabidopsis*. Plant J. *85*, 320–333.

Marschner, H., and Romheld, V. (1994). Strategies of plants for acquisition of iron. Plant Soil *165*, 261–274.

Mora-Macias, J., Ojeda-Rivera, J.O., Gutierrez-Alanis, D., Yong-Villalobos, L., Oropeza-Aburto, A., Raya-Gonzalez, J., Jimenez-Dominguez, G., Chavez-Calvillo, G., Rellan-Alvarez, R., and Herrera-Estrella, L. (2017). Malate-dependent Fe accumulation is a critical checkpoint in the root developmental response to low phosphate. Proc. Natl. Acad. Sci. USA *114*, E3563–E3572.

Müller, J., Toev, T., Heisters, M., Teller, J., Moore, K.L., Hause, G., Dinesh, D.C., Burstenbinder, K., and Abel, S. (2015). Iron-dependent callose deposition adjusts root meristem maintenance to phosphate availability. Dev. Cell *33*, 216–230.

Mussig, C., Shin, G.H., and Altmann, T. (2003). Brassinosteroids promote root growth in *Arabidopsis*. Plant Physiol. *133*, 1261–1271.

Noguchi, T., Fujioka, S., Choe, S., Takatsuto, S., Yoshida, S., Yuan, H., Feldmann, K.A., and Tax, F.E. (1999). Brassinosteroid-insensitive dwarf mutants of *Arabidopsis* accumulate brassinosteroids. Plant Physiol. *121*, 743–752.

Roschzttardtz, H., Conejero, G., Curie, C., and Mari, S. (2009). Identification of the endodermal vacuole as the iron storage compartment in the *Arabidopsis* embryo. Plant Physiol. *151*, 1329–1338.

Roschzttardtz, H., Conejero, G., Divol, F., Alcon, C., Verdeil, J.L., Curie, C., and Mari, S. (2013). New insights into Fe localization in plant tissues. Front. Plant Sci. *4*, 350.

Ruiz Herrera, L.F., Shane, M.W., and López-Bucio, J. (2015). Nutritional regulation of root development. Wiley Interdiscip. Rev. Dev. Biol. *4*, 431–443.

Sanchez-Calderon, L., Lopez-Bucio, J., Chacon-Lopez, A., Cruz-Ramirez, A., Nieto-Jacobo, F., Dubrovsky, J.G., and Herrera-Estrella, L. (2005). Phosphate starvation induces a determinate developmental program in the roots of *Arabidopsis thaliana*. Plant Cell Physiol. *46*, 174–184.

Santiago, J., Henzler, C., and Hothorn, M. (2013). Molecular mechanism for plant steroid receptor activation by somatic embryogenesis co-receptor kinases. Science *341*, 889–892.

Simon, M.L., Platre, M.P., Marques-Bueno, M.M., Armengot, L., Stanislas, T., Bayle, V., Caillaud, M.C., and Jaillais, Y. (2016). A PtdIns(4)P-driven electrostatic field controls cell membrane identity and signalling in plants. Nat. Plants *2*, 16089.

Singh, A.P., Fridman, Y., Friedlander-Shani, L., Tarkowska, D., Strnad, M., and Savaldi-Goldstein, S. (2014). Activity of the brassinosteroid transcription factors BRASSINAZOLE RESISTANT1 and BRASSINOSTEROID INSENSITIVE1-ETHYL METHANESULFONATE-SUPPRESSOR1/BRASSINAZOLE RESISTANT2 blocks developmental reprogramming in response to low phosphate availability. Plant Physiol. *166*, 678–688.

Singh, A.P., and Savaldi-Goldstein, S. (2015). Growth control: brassinosteroid activity gets context. J. Exp. Bot. *66*, 1123–1132.

Sun, Y., Fan, X.Y., Cao, D.M., Tang, W., He, K., Zhu, J.Y., He, J.X., Bai, M.Y., Zhu, S., Oh, E., et al. (2010). Integration of brassinosteroid signal transduction with the transcription network for plant growth regulation in *Arabidopsis*. Dev. Cell *19*, 765–777.

Sun, Y.D., Han, Z.F., Tang, J., Hu, Z.H., Chai, C.L., Zhou, B., and Chai, J.J. (2013). Structure reveals that BAK1 as a co-receptor recognizes the BRI1-bound brassinolide. Cell Res. *23*, 1326–1329.

Svistoonoff, S., Creff, A., Reymond, M., Sigoillot-Claude, C., Ricaud, L., Blanchet, A., Nussaume, L., and Desnos, T. (2007). Root tip contact with low-phosphate media reprograms plant root architecture. Nat. Genet. *39*, 792–796.

Szekeres, M., Nemeth, K., Koncz-Kalman, Z., Mathur, J., Kauschmann, A., Altmann, T., Redei, G.P., Nagy, F., Schell, J., and Koncz, C. (1996). Brassinosteroids rescue the deficiency of CYP90, a cytochrome P450, controlling cell elongation and de-etiolation in *Arabidopsis*. Cell *85*, 171–182.

Thomine, S., and Vert, G. (2013). Iron transport in plants: better be safe than sorry. Curr. Opin. Plant Biol. *16*, 322–327.

Ticconi, C.A., Lucero, R.D., Sakhonwasee, S., Adamson, A.W., Creff, A., Nussaume, L., Desnos, T., and Abel, S. (2009). ER-resident proteins PDR2 and LPR1 mediate the developmental response of root meristems to phosphate availability. Proc. Natl. Acad. Sci. USA *106*, 14174–14179.

Vragovic, K., Sela, A., Friedlander-Shani, L., Fridman, Y., Hacham, Y., Holland, N., Bartom, E., Mockler, T.C., and Savaldi-Goldstein, S. (2015). Translatome analyses capture of opposing tissue-specific brassinosteroid signals orchestrating root meristem differentiation. Proc. Natl. Acad. Sci. USA *112*, 923–928.

Vragovic, K., Bartom, E., and Savaldi-Goldstein, S. (2017). Quantitation of cell type-specific responses to brassinosteroid by deep sequencing of polysome-associated polyadenylated RNA. Methods Mol. Biol. *1564*, 81–102.

Wang, X., and Chory, J. (2006). Brassinosteroids regulate dissociation of BKI1, a negative regulator of BRI1 signaling, from the plasma membrane. Science *313*, 1118–1122.

Wang, Z.Y., Nakano, T., Gendron, J., He, J., Chen, M., Vafeados, D., Yang, Y., Fujioka, S., Yoshida, S., Asami, T., et al. (2002). Nuclear-localized BZR1 mediates brassinosteroid-induced growth and feedback suppression of brassinosteroid biosynthesis. Dev. Cell *2*, 505–513.

Ward, J.T., Lahner, B., Yakubova, E., Salt, D.E., and Raghothama, K.G. (2008). The effect of iron on the primary root elongation of *Arabidopsis* during phosphate deficiency. Plant Physiol. *147*, 1181–1191.

Wild, M., Daviere, J.M., Regnault, T., Sakvarelidze-Achard, L., Carrera, E., Lopez Diaz, I., Cayrel, A., Dubeaux, G., Vert, G., and Achard, P. (2016). Tissue-specific regulation of gibberellin signaling fine-tunes *Arabidopsis* iron-deficiency responses. Dev. Cell *37*, 190–200.

Williamson, L.C., Ribrioux, S.P., Fitter, A.H., and Leyser, H.M. (2001). Phosphate availability regulates root system architecture in *Arabidopsis*. Plant Physiol. *126*, 875–882.

Yin, Y., Wang, Z.Y., Mora-Garcia, S., Li, J., Yoshida, S., Asami, T., and Chory, J. (2002). BES1 accumulates in the nucleus in response to brassinosteroids to regulate gene expression and promote stem elongation. Cell *109*, 181–191.

Yu, X., Li, L., Zola, J., Aluru, M., Ye, H., Foudree, A., Guo, H., Anderson, S., Aluru, S., Liu, P., et al. (2011). A brassinosteroid transcriptional network revealed by genome-wide identification of BESI target genes in *Arabidopsis thaliana*. Plant J. *65*, 634–646.

Zanetti, M.E., Chang, I.F., Gong, F., Galbraith, D.W., and Bailey-Serres, J. (2005). Immunopurification of polyribosomal complexes of *Arabidopsis* for global analysis of gene expression. Plant Physiol. *138*, 624–635.

Zhu, J.Y., Li, Y., Cao, D.M., Yang, H., Oh, E., Bi, Y., Zhu, S., and Wang, Z.Y. (2017). The F-box protein KIB1 mediates brassinosteroid-induced inactivation and degradation of GSK3-like kinases in *Arabidopsis*. Mol. Cell *66*, 648–657.e4.

STAR★METHODS

KEY RESOURCES TABLE

REAGENT or RESOURCE	SOURCE	IDENTIFIER
Antibodies		
Rabbit polyclonal anti-BES1	(Yu et al., 2011)	N/A
Mouse monoclonal anti-Actin (plant) antibody	Sigma Aldrich	A0480; RRID: AB_476670
μMACS anti-GFP microbeads	Miltenyl Biotech	130-091-125
EZview ™ Red ANTI-FLAG ® M2 Affinity Gel	Sigma-Aldrich	F2426; RRID: AB_2616449
HIS-Select® Nickel Affinity Gel	Sigma-Aldrich	P6611
Mouse monoclonal anti-GFP antibodies	Sigma-Aldrich	11814460001; RRID: AB_390913
Bacterial and Virus Strains		
E. coli DH5α	ThermoFisher	18265017
Escherichia coli BL21 (DE3)	ThermoFisher	C600003
Agrobacterium tumefaciens (strain GV3101)	Savaldi-Goldstein's lab	N/A
Chemicals, Peptides, and Recombinant Proteins		
Brassinazole	(Asami et al., 2000)	N/A
Brassinolide	Chemiclones	N/A
K-ferrocyanide	Sigma Aldrich	4984
Na-azide	Alfa Aesar	26628-22-8
DAB	Roche	1171896001
Chloral Hydrate	Sigma Aldrich	15307
X-Glu	Thermo Scientific	R0851
IPTG	ORNAT Biochemicals	1758-1400
Complete protease inhibitor cocktail tablets	Sigma Aldrich	4693116001
MS salt	Duchefa Biochemie	M0222.0025
Plant Agar	Duchefa Biochemie	P1001.1001
Spectrum™ Plant Total RNA Kit	Sigma-Aldrich	STRN250-1KT
Immobilon-P PVDF Membrane	Merck Life Science	IPVH00010
Deposited Data		
Raw data and processed files for DNA sequencing	This study	GEO: GSE114250
Experimental Models: Organisms/Strains		
Arabidopsis thaliana: WT Col-0	N/A	N/A
Arabidopsis thaliana: bzr1-1D	(Wang et al., 2002)	N/A
Arabidopsis thaliana: bri1-116	*bri1* mutant collection in J. Chory lab (Li and Chory, 1997).	N/A
Arabidopsis thaliana: bri1 (GABI)	*bri1*(GABI_134E10), (Jaillais et al., 2011)	N/A
Arabidopsis thaliana (En2) bri1-6	(Yin et al., 2002)	N/A
Arabidopsis thaliana: lpr1	NASC	N653380
Arabidopsis thaliana: bki1-1	(Jiang et al., 2015)	N/A
Arabidopsis thaliana: cpd	(Szekeres et al., 1996)	N/A
Oligonucleotides		
Primers for cloning, genotyping, RT PCR and DNA binding assays	This paper, Table S5	N/A
Recombinant DNA		
pET28a-BZR1	This study	N/A
pET28a-BZR1-D	This study	N/A
pUBQ10-LPR1	This study	N/A
pLPR1-GUS	This study	N/A

(*Continued on next page*)

Continued		
REAGENT or RESOURCE	SOURCE	IDENTIFIER
CaMV35S-BKI1-YFP	(Wang and Chory, 2006)	N/A
pUBQ10-BKI1-mCHERRY	(Jaillais et al., 2011)	N/A
pHS-BKI1-mCitrine	This study	N/A
pBZR1-BZR1-CFP	(Wang et al., 2002)	N/A
pUBQ10-BES1-YPet	(Singh et al., 2014)	N/A
Software and Algorithms		
JMP	www.jmp.com	Version 10
NeuronJ: An ImageJ Plugin	https://imagescience.org/meijering/software/neuronj/	N/A
Other		
Spectrum™ Plant Total RNA Kit	Sigma-Aldrich	STRN250
High-Capacity cDNA Reverse Transcription Kit	ThermoFisher	4368814
On-Column DNase I Digestion Set	Sigma-Aldrich	DNASE70-1SET
Applied Biosystems® SYBR® Green PCR Master Mix	ThermoFisher	4309155

CONTACT FOR REAGENT AND RESOURCE SHARING

Further information and requests for resources and reagents should be directed to and will be fulfilled by the Lead Contact, Sigal Savaldi-Goldstein (sigal@technion.ac.il).

EXPERIMENTAL MODEL AND SUBJECT DETAILS

Plant Material, Growth Conditions and Treatments

All Arabidopsis (Arabidopsis thaliana) lines were in the Columbia-0 (Col-0) background, unless indicated otherwise. The following lines were used: *pUBQ10-BKI1-mCherry* and *bri1* (GABI_134E10) (Jaillais et al., 2011), *35S-BKI1-YFP* (Wang and Chory, 2006), *bki1-1* (Jiang et al., 2015), *pBZR1-BZR1-CFP* (Wang et al., 2002), *cpd*, *bri1-116, bri1-6* (in the En2 background) and *bzr1-D*. Seeds were sterilized as previously described (Fridman et al., 2014) and germinated on one-half-strength Murashige and Skoog medium supplemented with 0.2% (w/v) sucrose. Seedlings were transferred after 3-4 days (as specified for each experiment) to medium with either adequate (0.625 mM) or deficient (1μM) Pi levels, as previously described, (Singh et al., 2014) and analyzed after 4 additional days (unless specified otherwise). Chemical and hormone treatments were applied to 3-day-old seedlings, for 4 days, after which analysis was performed, unless otherwise stated. BRZ was added at a concentration of 3 μM. BL was added at a concentration of 2 nM unless indicated otherwise. For Fe-deficient medium, $FeSO_4$ was replaced with an equimolar concentration of $MgSO_4$. Quantification of P and Fe in the medium was performed by Inductively Coupled Plasma (ICP) analysis, as described in (Singh et al., 2014), Table S4. Seedlings were grown for 7 days (unless otherwise indicated), in 16h light (approximately 70 μmol m^{-2} s^{-1})/8h dark cycles, at 22°C.

METHOD DETAILS

RNA Extraction and Expression Analysis

RNA was isolated from the root tissues of 7-day-old seedlings. For quantitative analysis and RNA-seq, RNA extraction kit (Sigma-Aldrich) was used. RNA in association with polyribosomes was isolated as described in (Vragovic et al., 2017). Quantitative PCR was performed in an ABI 7300 PCR device (Applied Biosystems) using SYBR Green PCR Master Mix (Applied Biosystems). Primers used for the analysis are listed in Table S5.

Histochemical Detection and Light Microscopy

Histochemical detection of Fe was performed according to (Roschzttardtz et al., 2009). Briefly, 7-day-old seedlings were incubated for 30 min in Perls stain: 4% (v/v) HCl (Bio lab Ltd), 4% (w/v) K-ferrocyanide (Sigma-Aldrich). Seedlings were then washed with dH_2O and incubated for 1 h in DAB intensification solution (10 mM Na-azide and 0.3% (v/v) H_2O_2 in methanol). Subsequently, seedlings were washed with Na-phosphate buffer (pH 7.4) and incubated in 0.025% (w/v) DAB (Roche) and 0.005% (v/v) H_2O_2 for 2 min. The reaction was then stopped by washing with dH_2O, before transferring the root to a clearance solution comprised of chloral hydrate (1 g/ml) and 15% glycerol. Anatomical sectioning of roots was performed after histochemical detection of Fe, as described in (Fridman et al., 2016), but without adding a dye to the fixative. Histochemical detection of GUS staining was performed as previously described (Hacham et al., 2011). Five-day-old seedlings were transferred to an appropriate MS medium containing 3 μM BRZ or freshly prepared $FeSO_4$ as indicated, for 48 h prior to GUS staining. Images were captured with an AxioImager microscope (Zeiss).

Protein Extraction and Western Blotting

Roots of 7-day-old seedlings were harvested and 100 mg root tissue was crushed in liquid nitrogen. Powder from root tissues was dissolved in with protein extraction buffer (50 mM Tris HCl, pH 6.8, 150 mM NaCl, 1 mM EDTA, pH 8, 0.5% SDS and 1% protease inhibitor cocktail (Sigma) and then centrifuged (5 min, 12000 rpm, 4°C). Equal amounts of supernatant (30 μL) from each treatment were mixed with Laemmli buffer, separated by 10% SDS PAGE, and transferred to a PVDF membrane (Millipore, 300mA, 1h). After transfer, the PVDF membrane (Millipore) was incubated overnight (4°C, 50 rpm) in 0.5% Phosphate Buffered Saline Tween-20 (PBST) containing 1% milk. The membrane was then incubated with primary anti-BES1 antibodies (diluted 1:1000, 2 h, 60 rpm, room temperature), washed 3 times in 0.5% PBST and incubated for 1 h with anti-rabbit-HRP secondary antibodies (Abcam). The blot was developed using ECL reagents. Immunoreactive bands were documented using LAS400 software. The pBES1/BES1 ratio was calculated using the ImageJ gel analysis tool. The pBES1/BES1 ratio measured under adequate conditions was set to 1 and the ratios for the other treatments were normalized accordingly. For BKI1-YFP immunoprecipitation, 300 mg root tissue used and the extracted proteins were incubated with μMACS anti-GFP microbeads (Miltenyl Biotech). Western blot was probed with anti-GFP antibodies and with anti-actin for internal control.

DNA Binding Measurements by Fluorescence Anisotropy

dsDNA for the binding reaction was prepared using the oligomers shown in Table S5, by hybridization of 20 μM final concentration DNA in TAE buffer (5 mM NaCl and 12.5 mM $MgCl_2$), at 85°C for 3 minutes, followed by slow cooling to room temperature before storage at -20°C. DNA binding measurements were performed with a PC1 spectrofluorimeter (ISS, Champaign, IL) set to a T-format configuration for simultaneous acquisitions on two emission channels, using monochromators equipped with automatic polarizers. Samples were equilibrated (60 min, room temperature) and then measured at $\lambda_{ex} = 492$ nm, using vertical polarized light. The emitted vertical and horizontal polarized light was monitored at 90° with emission monochromators at $\lambda_{em} = 525$ nm. The G-factor for correction of the different gain between vertical and horizontal PMT detectors was calculated as described by the manufacturer.

Our binding model for DNA substrates to BZR1 is described by the following stoichiometric reaction:

$$\mathrm{BZR1} + dsDNA \overset{K_D}{\longleftrightarrow} \mathrm{BZR1} \cdot dsDNA$$

$$K_D = \frac{[\mathrm{BZR1} \cdot dsDNA]_{eq}}{[\mathrm{BZR1}]_{eq}[dsDNA]_{eq}}$$

When $[\mathrm{BZR1}]_T \ll [DNA]_T$ then the general solution for this equilibrium binding scheme is in the form of the following Equation 1:

$$Normalized\ Fraction\ Bound = \frac{[\mathrm{BZR1}]}{[\mathrm{BZR1}] + K_D} \quad \text{(Equation 1)}$$

Since the observed change in the fluorescence total intensity (FTI) was negligible throughout the measurements, the FA could be fitted directly to Equation 1 without correcting for changes in FTI. Binding curves were fitted to Equation 1 using NNLS via MATLAB (cftool).

Live Imaging and Confocal Microscopy

A confocal laser-scanning microscope LSM 510 META (Zeiss) equipped with a 25X water immersion objective lens (NA 0.8) was used to determine the localization of BKI1-mCHERRY, BKI1-YFP, BES1-YPet and BZR1-CFP. Roots were imaged in water in the presence or absence of 10 mg/mL propidium iodide (PI). PI and YFP were viewed at excitation wavelengths of 561 nm and 488 nm, respectively. Fluorescence emission was collected at 575 nm for PI and cherry, and with a 500 and 530 nm bandpass for YFP and YPet. CFP was viewed by using TiSapphier multiphoton laser at excitation wavelength of 870 nm and emission wavelength of 465nm.

Heat Shock of *pHS-BKI1-mCitrine*

7-day-old seedlings were transferred to optical plates (Ibidi, 35 mm μ-dish) and covered with MS medium containing the indicated Pi and Fe availability as indicated in the main text. The plates were sealed using paraffin and incubated in a 37°C for 30 min in a pre-heated water bath. Plates were then imaged using an LSM 710 confocal microscope (ZEISS) at the indicated intervals. BKI1-mCitrine was viewed at excitation wavelengths of 514 nm and the signal was channeled through a BP495-550 GaAsP detector.

Constructs and Transgenic Lines

The full-length coding sequence of *LPR1* was amplified from Arabidopsis cDNA and cloned to the polylinker of pBJ36 containing the pUBQ10 promoter. The promoter fragment, 2282 bp upstream of *LPR1* coding sequences, was amplified from genomic DNA and cloned to the polylinker of pBJ36 containing the β-glucuronidase plus (GUS-plus) reporter gene. *pUBQ10-LPR1* and *pLPR1-GUS* fragments were then subcloned into the binary vector pART27. *pHS-BKI1-mCitrine* was cloned using multisite gateway LR cloning with the HSprom/pDONRP4P1R (Marques-Bueno et al., 2016), BKI1/pDONR221 and mCITRINE/pDONRP2RP3 entry vectors (Jaillais et al., 2011) and pB7m34GW destination vector (Karimi et al., 2007). Plant transformation was performed with the Agrobacterium-mediated floral dip transformation method. Primers used for cloning are listed in Table S5.

QUANTIFICATION AND STATISTICAL ANALYSIS

Sequencing and Data Analysis

8 samples of mRNA (wild type and *bzr1-D*, following 24 hours of -Pi+Fe, in two biological repetitions), were collected from roots of 7-day-old seedlings. Samples were sequenced at the Technion Genome Center on an Illumina HiSeq 2500, to obtain 50 bp single end reads (Vragovic et al., 2015). These reads were aligned to the TAIR10 assembly of the Arabidopsis thaliana genome, using Tophat2 v2.0.11. Transcript coordinates from the TAIR10 reference set were used to guide the alignment process. After alignment, the numbers of reads per gene were estimated using HTSeq v0.6.1. DESeq2 v1.2.8 was used to normalize read counts and perform pairwise differential expression analysis. Gene sets were identified based on their differential expression. Significantly modulated genes were considered with a fold change of 1.5 in response to low Pi and adjusted p-value (false discovery rate) of 0.1.

Analysis of Physiological Measurements

Data was analyzed by one-way analysis of variance (ANOVA) using JMP version 10 software (SAS Institute, Cary, NC, USA). Differences between treatments were determined by Student's t test. In multiple comparisons, Tukey–Kramer HSD test ($p \leq 0.05$) was implemented. In the measurements where variances were unequal (Figures 1A, 1C, 3B, 4C, 4D, and 4G), Tukey–Kramer HSD test was performed on ranked data ($p \leq 0.05$). Results are shown in Table S6.

DATA AND SOFTWARE AVAILABILITY

RNA-seq data have been deposited into the Gene Expression Omnibus (GEO: GSE114250).